Nanoparticles Based on Star Polymers as Theranostic Vectors: Endosomal-Triggered Drug Release Combined with MRI Sensitivity

Yang Li, Hien T. T. Duong, Sophie Laurent, Alexandre MacMillan, Renee Megan Whan, Luce Vander Elst, Robert N. Muller, Jinming Hu, Andrew Lowe, Cyrille Boyer, and Thomas P. Davis**

Dual-functional star polymers (diameters 15 nm) are synthesized producing nanoparticles with excellent colloidal stability in both water and serum. The nanoparticles are built with aldehyde groups in the core and activated esters in the arms. The different reactivity of the two functional groups to sequentially react with different amino compounds is exploited; doxorubicin (DOX) and 1-(5-amino-3-aza-2-oxypentyl)-4,7,10-tris(*tert*-butoxycarbonylmethyl)-1,4,7,10-tetraazacyclododecane (DO3A-*t*Bu-NH_2)—a chelating agent effective for the complexation of Gadolinium ions (Gd). The activated ester group is employed to attach the DO3A chelating agent, while the aldehyde groups are exploited for DOX conjugation, providing a controlled release mechanism for DOX in acidic environments. DOX/Gd-loaded nanoparticles are rapidly taken up by MCF-7 breast cancer cells, subsequently releasing DOX as demonstrated using in vitro fluorescence lifetime imaging microscopy (FLIM). Endosomal, DOX release is observed, using a phasor plot representation of the fluorescence lifetime data, showing an increase of native DOX with time. The MRI properties of the stars are assessed and the relaxivity of Gd loaded in stars is three times higher than conventional organic Gd/DO3A complexes. The DOX/Gd-conjugated nanoparticles yield a similar IC_{50} to native DOX for breast cancer cell lines, confirming that DOX integrity is conserved during nanoparticle attachment and release.

1. Introduction

Theranostics, a combination of drug delivery and imaging, is an emerging field, as progress could potentially lead to triggered drug release at precise physical locations (tracking), and provide instantaneous feedback on physical responses to delivery events. Building responses to different delivery vectors using a range of imaging techniques, for example, computer tomography (CT), magnetic resonance imaging (MRI), positron emission tomography (PET), and fluorescence imaging has been described in pioneering recent work.[1] MRI responsiveness remains an attractive target for theranostic nanoparticle design, as MRI scanners are readily available in large public hospitals, and MRI scans do not subject patients to ionizing radiation. Two different types of MRI contrast agents (CAs) are commonly employed to build theranostic devices; both CAs have the ability to shorten the surrounding water protons longitudinal

Y. Li, Prof. A. Lowe, Prof. C. Boyer
Centre for Advanced Macromolecular Design (CAMD)
School of Chemical Engineering
University of New South Wales
Sydney, New South Wales 2052, Australia
E-mail: cboyer@unsw.edu.au
Y. Li, Dr. H. T. T. Duong, Prof. C. Boyer
Australian Centre for Nanomedicine
School of Chemical Engineering
University of New South Wales
Sydney, New South Wales 2052, Australia
Dr. S. Laurent, Prof. L. V. Elst, Prof. R. N. Muller
NMR and Molecular Imaging Laboratory
Department of General
Organic and Biomedical Chemistry
University of Mons
7000, Mons, Belgium
Dr. A. MacMillan, Dr. R. M. Whan
Biomedical Imaging Facility
University of New South Wales
Sydney, New South Wales 2052, Australia
Prof. R. N. Muller
CMMI – Center of Microscopy and Molecular Imaging
Rue Adrienne Bolland, 8
B-6041, Gosselies, Belgium
Dr. J. Hu, Prof. T. P. Davis
ARC Centre of Excellence in Convergent Bio-Nano
Science & Technology
Monash Institute of Pharmaceutical Sciences
Monash University
Parkville, Victoria 3052, Australia
E-mail: Thomas.p.davis@monash.edu
Prof. T. P. Davis
Department of Chemistry
University of Warwick
Coventry CV4 7AL, UK

DOI: 10.1002/adhm.201400164

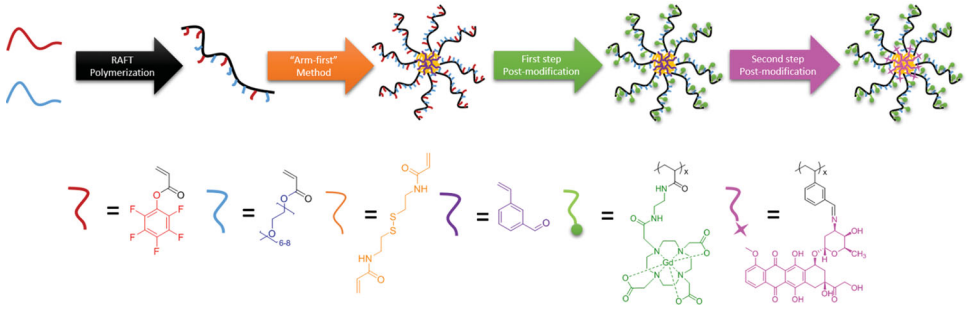

Scheme 1. Schematic representation of the synthesis of multifunctional core cross-linked star polymers using sequential postmodification.

(T_1) and transversal (T_2) relaxation time to improve MRI contrast. Gadolinium-based CAs yield positive contrast as indicated by an increase in image brightening, while, in contrast, iron oxide nanoparticle-based CAs provide a negative contrast—leading to image darkening.[2] Presently, the most commonly employed CAs in the clinic is based on gadolinium (Gd). As Gd is highly toxic, Gd is chelated with small organic compounds to maintain solution stability while obviating direct interactions of Gd with biological media.[3] Small organic CAs have a number of shortcomings: i) a short biocirculation times, ii) low contrast at high magnetic fields, and iii) systemic delivery (nonspecificity). Recent published work on incorporating Gd into polymeric nanostructures has provided some encouragement that nanoparticle-based CAs can overcome the present application drawbacks.[4] Polymeric nanoparticles can be easily tuned to produce sizes from 10 to 200 nm with bespoke morphologies, potentially to take advantage of the enhanced permeation retention (EPR) effect, for enhanced targeting. In addition, polymeric nanoparticles can be easily decorated with targeting moieties to further improve specific targeting, and they can encapsulate a greater number of Gd per nanoparticles to enhance local contrast.[5] In another significant advantage, encapsulating Gd in nanoparticle structures reduces molecular tumbling, significantly increasing the relaxivity of Gd at high magnetic fields. In previous work, we demonstrated that the relaxivity values of Gd could be multiplied three times when encapsulated in a core cross-linked polymer nanogel.[4a] Finally, the encapsulation of therapeutic compounds, such as doxorubicin, in polymeric nanoparticles have proven superior therapeutic efficacy in comparison to single therapeutic compounds in in vitro[6] and in vivo[7] for the treatment of various cancers. The main advantages of using polymeric nanoparticles for drug delivery applications are to increase the aqueous solubility of the therapeutic drugs, to limit the drug degradation by enzymatic reactions and to improve the bioavailability of therapeutic compounds. In addition, the use of biodegradable materials for the preparation of the nanoparticles allows sustained drug release within the target sites over a period of days.

In this present work, we extend our previous work on the use of core cross-linked star (CCS) polymers as MRI nanoparticulate CAs to reversibly store and deliver a common chemotherapy drug (doxorubicin). In a versatile (and novel) synthetic strategy, we exploit two different functional groups within the nanoparticle structure to allow sequential postmodification of the stars, thereby introducing both Gd chelating agent and doxorubicin (DOX). We adopted both activated ester chemistry[8] and reversible imine bond formation using aldehyde groups.[6,9]

2. Results and Discussion

2.1. Synthesis of CCS Polymers

CCS polymers containing a water-soluble segment of poly(ethylene glycol) and functional groups were prepared using an "arm-first" method developed by our group.[10] Poly(ethylene glycol) segments were incorporated to imbue water solubility, while pentafluorophenyl acrylate and vinyl benzyl aldehyde were introduced to conjugate both a chelating agent and chemotherapy drugs. First, a copolymer comprised of poly(ethylene glycol) methyl ether acrylate (PEGA) and an activated ester monomer—pentafluorophenyl acrylate (PFPA)—was synthesized via reversible addition fragmentation transfer (RAFT) polymerization (**Scheme 1**).[11] Kinetic studies evidenced that PFPA was consumed faster than PEGA in the polymerization,[12] leading to a gradient copolymer rich in PFPA at the α-end. This gradient result was favorable for our purpose since this increased the PFPA concentration in the star arms, exposing the Gd chelates to water molecules, enhancing water relaxivity properties. Subsequently, P(PEGA-*stat*-PFPA) copolymers were chain extended in the presence of both a cross-linker (*N,N*-bis(acryloyl)cystamine) and vinyl benzyl aldehyde (VBA) to generate CCS polymers (**Table 1**). GPC traces confirmed the synthesis of well-defined CCS polymers with high-molecular-weight distributions. Free arms (around 20%) were then completely eliminated by precipitation in mixture diethyl ether and dichloromethane, finally yielding well-defined stars with PDIs lower than 1.2 (**Figure 1**). Subsequently, the stars were analyzed by ^{1}H and ^{19}F NMR

Table 1. Polymers used in this study.

	$\bar{M}_{n,\,SEC}$ [a)] [g mol^{-1}]	$Đ_m$ [a)]	F_{PEGA} [b)] [%]	F_{PFPA} [b)] [%]	F_{VBA} [b)] [%]
P(PFPA-*stat*-VBA)	9000	1.16	–	51	49
CCS polymers	84 000	1.16	42	34	24

[a)]Molecular weight and dispersity determined by GPC; [b)]Molar composition of the linear polymer and core cross-linked star (CCS) polymer determined by ^{1}H and ^{19}F NMR analysis.

Adv. Healthcare Mater. **2014**,
DOI: 10.1002/adhm.201400164

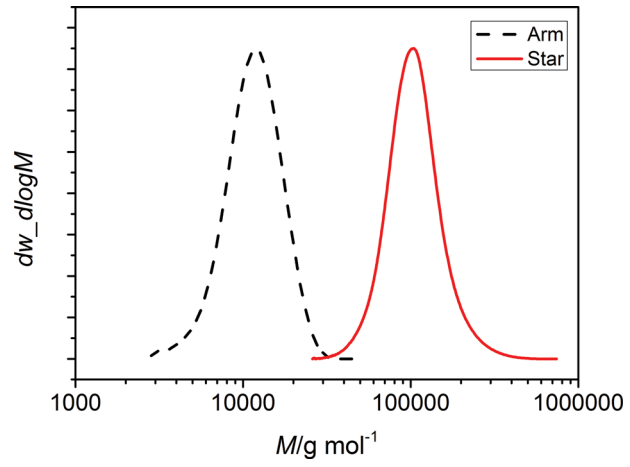

Figure 1. GPC analyses of (- -) P(PEGA-*stat*-PFPA) linear arm and (—) purified P(PEGA-*stat*-PFPA-*stat*-VBA) CCS polymer.

analyses. The presence of vinyl benzyl aldehyde groups was confirmed by signals at 6.8–7.4 and 9.9 ppm (aromatic and aldehyde groups, respectively) (**Figure 2**A). The compositions of the CCS polymers are reported in the Supporting Information.

2.2. Conjugation of DO3A and Doxorubicin onto CCS Polymers

Subsequently, the presence of the two reactive groups (aldehyde and pentafluoro-activated ester) was exploited to sequentially introduce functionality to the star structures. Two different amino compounds, that is, 1-(5-amino-3-aza-2-oxypentyl)-4,7,10-tris(*tert*-butoxycarbonylmethyl)-1,4,7,10-tetraazacyclododecane (DO3A-*t*Bu-NH_2) and doxorubicin, were reacted concurrently. First, DO3A-*t*Bu-NH_2 was reacted with pentafluorophenyl ester acrylate groups using an equimolar ratio, that is, [PFPA]:[DO3A] = 1:1. ^{1}H and ^{19}F NMR analyses confirmed that the reaction between DO3A-*t*Bu-NH_2 and PFP group was selective and quantitative (Figure 2B). Pentafluorophenol was released, after reaction, exemplified by the signals at −166, −172, and −186 ppm. Interestingly, the signal attributed to the aldehyde groups (at 9.9 ppm) was not altered after reaction with DO3A-*t*Bu-NH_2 (Figure S10, Supporting Information), demonstrating that the reaction between DO3A-*t*Bu-NH_2 and the PFP group is selective. Next, the *tert*-butyl group was cleaved using trifluoroacetic acid (TFA), as monitored by ^{1}H NMR analysis to follow the disappearance of the signal at 1.4 ppm (Figure 2C). Importantly, the aldehyde signal stayed unreacted, available for further reaction. Then, the stars were incubated in the presence of Gd under slightly basic conditions

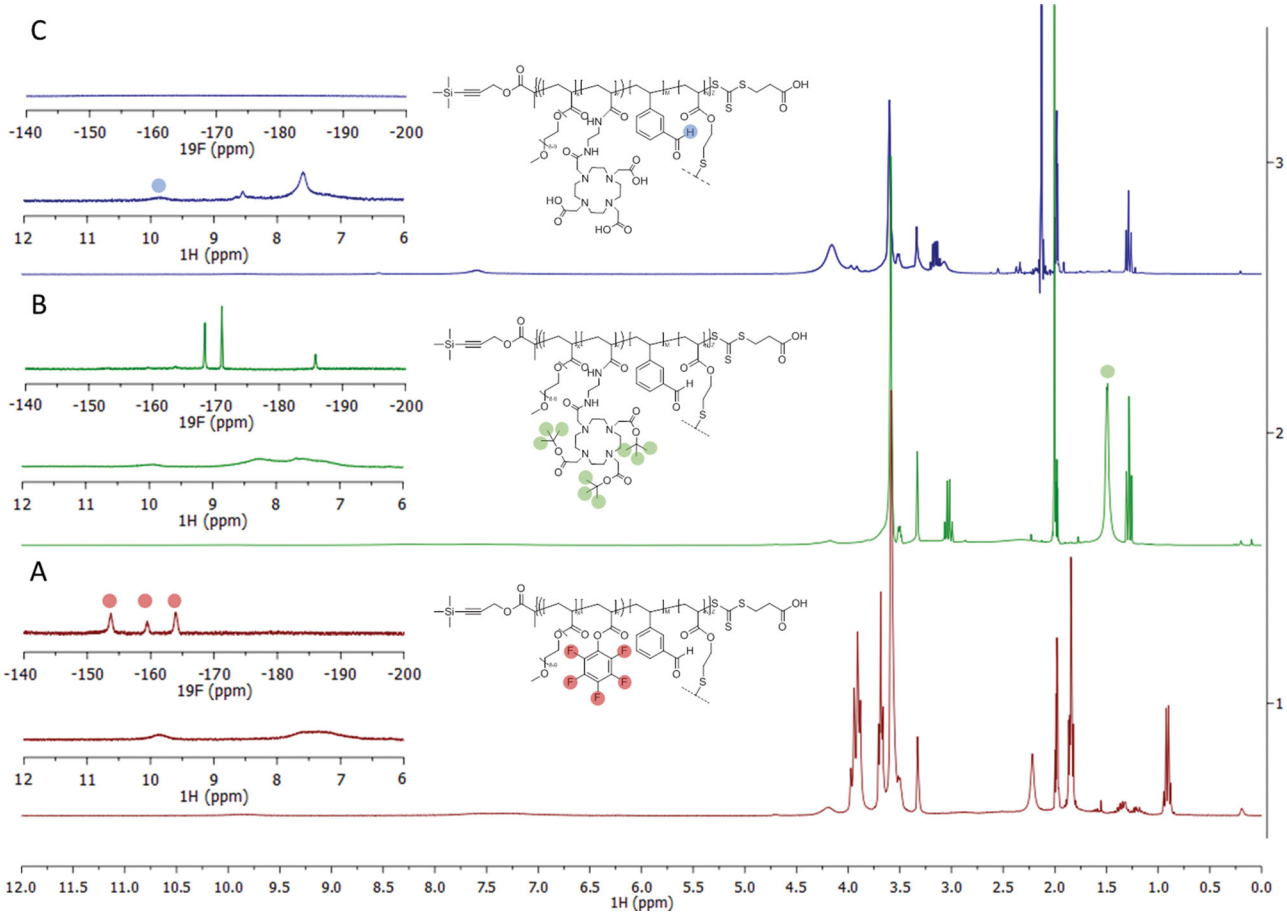

Figure 2. ^{1}H NMR spectra of A) core cross-linked star (CCS) polymers containing aldehyde and pentafluorophenyl-activated ester; B) CCS polymers after attachment of DO3A-*t*Bu-NH_2, C) CCS polymers after hydrolysis of *tert*-butyl group into carboxylic acid group.

(pH 8) for 24 h to facilitate complexation. Finally, the stars were then purified by dialysis until all the excess of Gd was eliminated. The yield of complexed-Gd was estimated to be around ≈95% using ICP-OES, in accord with previous observations published on a similar system.[4a]

Finally, the unreacted aldehyde groups in the star cores were exploited in a condensation reaction to conjugate doxorubicin (DOX) via Schiff base/imine bonds. The imine bond is reversible as it can be hydrolyzed in acidic media, reforming the aldehyde, providing a facile mechanism for the pH-stimulated release of DOX.[13] The condensation reaction was performed in a DMSO–water mixture (50/50 v-v) at room temperature in the presence of triethylamine. After reaction, the stars were purified using dialysis against DMSO, and then against water, to yield dark-red solutions. As a control experiment, doxorubicin was physically loaded into nonfunctional stars, and purified using the same process. After dialysis, the control solution proved colorless, confirming that DOX has been completely removed when only physically bound (data not shown). Subsequently, UV–vis analyses were used to assess the doxorubicin conjugation efficiency via a preconstructed calibration curve (Figure S13, Supporting Information). DOX concentrations loaded in the stars (after purification) could be calculated from the absorbance peak at 490 nm, using the following equation: $[DOX] = \lambda^{490}/(\epsilon^{490} \times l)$, with λ^{490}, ϵ^{490}, and l correspond to intensity of absorbance peak at 490 nm, extension coefficient of doxorubicin at 490 nm, and path length, respectively.[9a] The conjugation reaction yields (calculated by the following equation: yield (%) = [DOX]/[VBA], with [DOX] and [VBA] stand for doxorubicin and VBA concentration, respectively) proved to be very high (yield ≈80%), that is, 80% of the aldehyde groups were reacted with DOX. The amount of doxorubicin loaded in the star polymers could be easily tuned by controlling the amount of VBA present in the cores.

DLS was used to determine the sizes of the star polymers dispersed in water, before and after DOX and Gd conjugation. DLS analyses show a slight increase in star size after doxorubicin conjugation ($size^{DLS}$ = 15 nm) without any significant changes to the size distribution (D ≈ 0.1). Transmission electron microscopy analyses confirmed nanoparticle sizes around 15 nm, in accord with the DLS data (Figure S14, Supporting Information). It is noteworthy that doxorubicin/Gd-loaded star polymers could be freeze-dried and redispersed in water without any identifiable size changes. In summary, the conjugated stars display high stabilities in serum, a tuneable drug-loading capacity, a controlled release mechanism, and high reproducibility on freeze-drying.[14]

2.3. Physicochemistry Characterization of CCS Polymers Loaded with Gd and Doxorubicin

The release of DOX from the star polymers was investigated under different pH conditions (pH 7.5, 6.5, 6.0, and 5.5) using fluorescence spectroscopy. The data in **Figure 3** show the rate of doxorubicin release with time. At pH 7.0 (close to blood pH), doxorubicin release was very slow (after 24 h, only 20% of doxorubicin had been released from the stars). At, pH 5.5–6.0 corresponding to the pH of the endosome or tumor

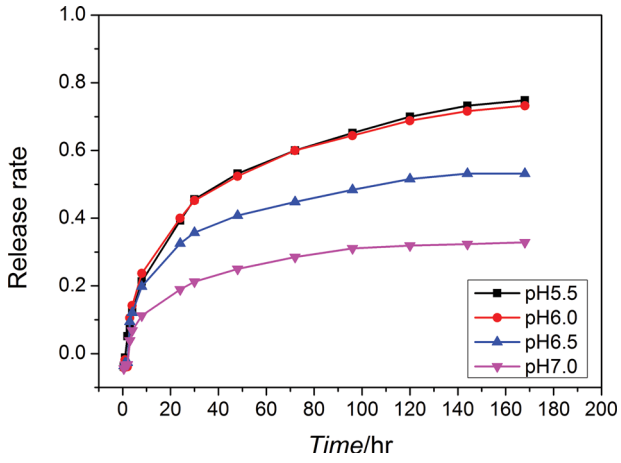

Figure 3. Cumulative DOX release profiles from the star polymers incubated in different pH buffers.

tissue doxorubicin was released relatively quickly with 60% of free doxorubicin evident after 24 h. The integrity of DOX after release was confirmed by mass spectrometry and fluorescence spectroscopy evidencing the absence of DOX degradation during the functionalization and release processes. In addition, a fluorescence study confirmed the structure of doxorubicin after release from the star polymers (Figure S15, Supporting Information).

2.4. In Vitro Cytotoxicity and Intracellular Drug Release Study Using Confocal Microscopy and Fluorescence Lifetime Imaging Microscopy

We subjected the Gd- and DOX-loaded stars to in vitro testing using two different cell lines: MRC-5 lung fibroblast cells and MCF-7 breast cancer cells. Star polymers (without doxorubicin and Gd) and Gd-loaded star polymers (without DOX) proved noncytotoxic (below 10 mg mL^{-1}) to both cell lines (data not shown), in accord with our previous study on the toxicity of P(OEGA)-based polymers prepared by RAFT polymerization.[9,15] The toxicity data for DOX- and Gd-conjugated stars confirmed an IC_{50} close to the toxicity of native DOX after 72 h for cancer cells. In contrast, DOX/Gd-loaded stars presented a lower toxicity to normal cells (**Table 2**). Our results showing a difference of toxicity between DOX-loaded nanoparticles and native DOX are in accord with previous publications.[9a,15,16]

The toxicity of the Gd/DOX-loaded stars can be explained by the release of doxorubicin and its subsequent accumulation in

Table 2. Comparison of IC_{50}($\times 10^{-6}$ M) values for doxorubicin and doxorubicin/Gadolinium-loaded star polymers for MRC-5 normal fibroblast cells and MCF-7 breast cancer cells ($n = 3$).

	IC_{50} [$\times 10^{-6}$ M]	
Cell line	Free DOX	Star-DOX
MRC-5	0.605 ± 0.064	0.952 ± 0.163
MCF-7	0.082 ± 0.011	0.084 ± 0.011

Adv. Healthcare Mater. 2014,
DOI: 10.1002/adhm.201400164

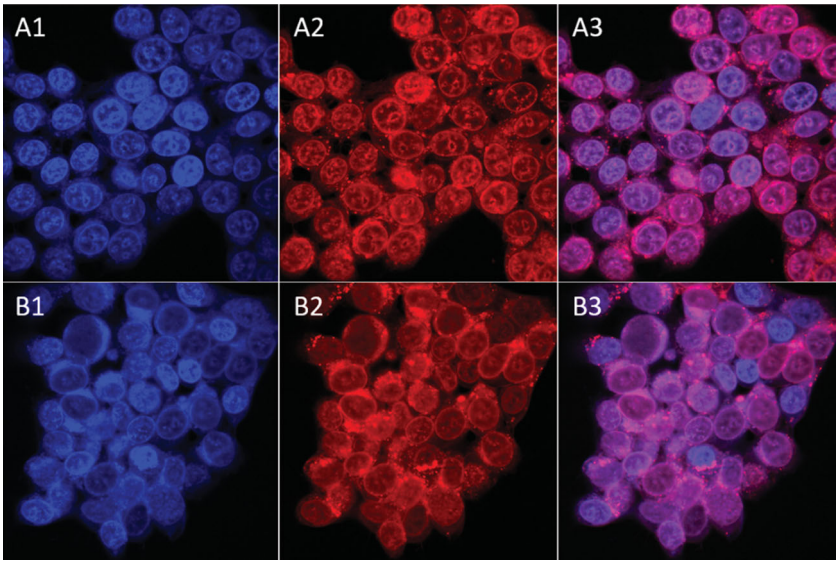

Figure 4. Confocal microscopy after 24 h incubation of A) DOX/Gd-loaded star polymers and B) native DOX; 1) DAPI-stained nuclei, 2) DOX channel, 3) merged DAPIDOX channel. DOX fluorescent images were acquired at $\lambda^{ex} = 485$ nm and $\lambda^{em} = 595$ nm. (Note: DOX concentration was fixed at 0.5×10^{-6} M for all the experiments).

the nucleus of the cells as confirmed by confocal microscopy measurements. An established mechanism of chemotherapy action of DOX depends on the accumulation of DOX in the nucleus of cells damaging the DNA, ultimately resulting in cell death. **Figure 4** shows different confocal microscopy images taken after 24 h for both Gd/DOX-loaded stars and native DOX. The nucleus was stained by DAPI to help the visualization of DOX localization in the cells. Confocal microscopy images indicate a slow accumulation of DOX (Gd/DOX-loaded star) in the nucleus after 5 h (Figure S16, Supporting Information) with a total accumulation after 24 h (Figure 4) for Gd/DOX-loaded stars (native DOX was seen to accumulate rapidly in the nucleus). In conclusion, the confocal microscopy suggests a high cell uptake for the Gd/DOX-loaded star in MCF-7.

We are currently investigating the mechanism of cell uptake of these nanoparticles. However, previous publications using PEG-coated nanoparticles have also reported a high cell uptake in cancer cells and non-cancerous cells via a clathrin-independent endocytosis pathway. For example, Yang and co-workers[17] have investigated the cell uptake of PEG-coated nanoparticles and have demonstrated a caveoleo-dependent pathway, but clathrin-independent endocytosis was involved in the uptake of PEG polymeric micelles in a human ovarian cell line (A2780). However, it has been well established that the specific endocytic pathway responsible for uptake of a nanocarrier can vary greatly and can be dependent on not only cell type, but also the physicochemical properties of the nanocarrier such as size, shape, surface chemistry, and charge, among others.[18]

To probe intracellular release of DOX from star polymers, we invoked fluorescence lifetime imaging microscopy (FLIM),[9b,15,19] as FLIM is a powerful tool for monitoring dynamic intracellular DOX release from polymeric nanoparticles.[9a,19a,20] The fluorescence lifetime of a fluorophore corresponds to the average time a molecule stays in its excited state before returning to the ground state. In general, the fluorescence lifetime is critically dependent upon the physicochemical environment that surrounds the fluorescent probe.[21] FLIM provides an intensity-independent measurement, and in the context of this work, FLIM can be used to monitor the changes in DOX fluorescence lifetimes based on the DOX nanoenvironment. In our work, we could distinguish four different DOX environments using FLIM measurements: i) native (free) DOX in media, ii) DOX conjugated to the stars in media, iii) native DOX released from pH-responsive stars in the cellular organelles, and iv) DOX conjugated to stars in the cellular organelles. The fluorescence lifetimes in aqueous solution were first measured using time-correlated single-photon counting (TCSPC). The concentration-independent single-exponential decay corresponding to a lifetime of 1.0 ns for native (free) DOX is consistent with the known published lifetime values,[19a] and an average lifetime of 4.0 ns was determined for DOX-loaded stars. An increase in DOX fluorescence lifetime has been previously observed for DOX encapsulated in polymeric nanoparticles.[9a,19a,20a] The fluorescence lifetimes of native DOX and DOX/Gd-loaded stars are substantially different, enabling differentiation in solution, making FLIM ideal for monitoring intracellular DOX release from star polymers.

FLIM was then performed using native DOX and DOX/Gd-loaded stars in a MCF-7 breast cancers cell line (at a concentration of 0.5×10^{-6} M based on DOX). **Figure 5** shows the FLIM images and lifetime distributions taken from cells treated with native DOX and with DOX-loaded stars after 1 h. **Figure 6** shows the fluorescence lifetime distribution of DOX/Gd-loaded stars in MCF-7 cells for 1, 5, and 24 h of incubation. The lifetime of DOX increased to 2 ns in the nuclei in contrast with its corresponding value in media solution (1.0 ns). The increased lifetime of DOX in the nuclei can be attributed to the well-accepted DOX–DNA intercalation process that subsequently induces apoptotic cell death. We observed a bimodal lifetime distribution in the MCF-7 cell line when treated with DOX/Gd-loaded stars over time. The increase in shorter lifetime components is consistent with the release of DOX from DOX/Gd-loaded stars. FLIM measurements can be used to reliably distinguish and detect both native DOX and DOX/Gd-loaded stars in the same voxel (otherwise hampered by the overlapping fluorescence emission spectra).

As demonstrated in Figure 3, DOX release from DOX-loaded stars can be easily monitored in buffered model reactions, evidencing the effect of pH on release, via the breakage of imine bonds. However, while useful, the model reactions provide no guarantee of intracellular bond breakage and subsequent DOX release. This motivated us to expand our DOX fluorescence lifetime over periods of time using MCF-7 live cells. As incubation time increased, we observed a significant decrease in the proportion of ≈4.6 ns lifetime contribution. However, primary FLIM

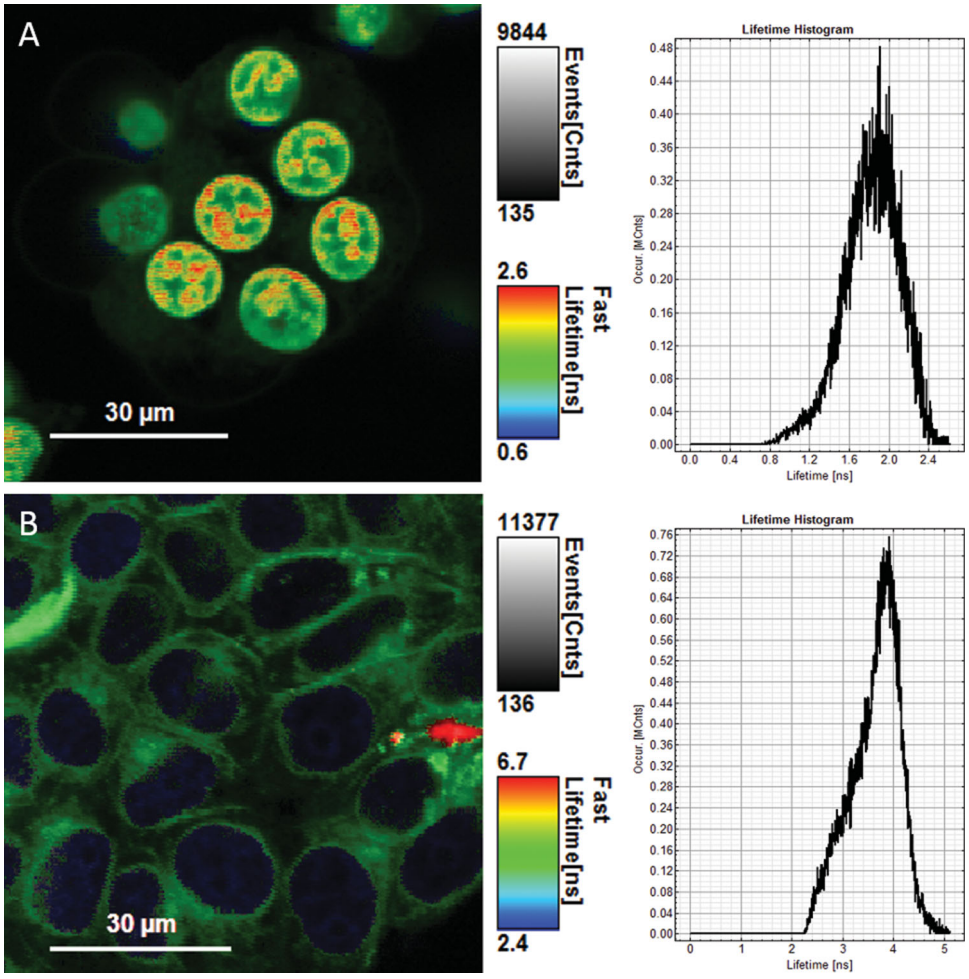

Figure 5. FLIM images and a histogram showing data for cells treated with A) native DOX and B) DOX/Gd-loaded stars after 1 h in media solution containing MCF-7. The FLIM image denotes the fluorescence lifetimes measured at each pixel and displayed as color contrast image. The corresponding false-color look-up table represents the lifetime distribution.

data allow for only a qualitative measurement. FLIM data can be manipulated to yield a phasor plot analysis, which presents the fluorescence lifetime data in a graphical form, negating the need for exponential fitting to the fluorescence decay.[22] Phasor plotting was originally developed to overcome some of the drawbacks of FLIM, such as the low photon counts per pixel, which renders differentiation between one and two lifetimes difficult.[22c] In the phasor analysis of lifetime images, lifetime data at each pixel are transformed. All single-exponential lifetimes lie on a universal circle, while multi-exponential lifetimes are a linear combination of their components (**Figure 7**). The first successful use of phasor plot analysis to study DOX release from dextran nanoparticles was recently reported by our group.[9b] As seen in Figure 7C, the longer fluorescence lifetime contribution to the phasor plot (highlighted in red) is predominant after 1 h of DOX/Gd-loaded star incubation in MCF-7 cells. Over 24 h of incubation, there is a time-dependent shift to shorter fluorescence lifetimes (highlighted in green (5 h) and orange (24 h)). This phasor plot shift indicates that there is an increase in the fractional contribution to fluorescence from released (free) DOX over time. In addition, FLIM images for MCF-7 cells demonstrate an increasing concentration of released DOX with shorter fluorescence lifetime in the nucleus (Figure 7A) analogous with the free DOX cell uptake behavior (Figure S17, Supporting Information). This result suggests that a high fraction of DOX is released from the star polymers (approximately 90%) after 24 h, in contrast to the model release profile performed at different pH in model solutions, where only 60% was observed at pH 5.5 after 24 h (Figure 3). This difference obtained between model release and in vitro measurement can be explained by the presence of other mechanisms of release in the cells, including enzymatic reactions. The FLIM results support our cytotoxicity results in MCF-7, where we observed a similar toxicity for MCF-7 using both native DOX and DOX-loaded star polymers.

2.5. MRI Contrast Agent Relaxivity Measurements

To determine the efficacy of Gd-star-positive contrast agents, the nuclear magnetic field relaxation dispersion (NMRD) profiles of Gd-loaded stars and Gd/DOX-loaded stars were measured

Adv. Healthcare Mater. **2014**,
DOI: 10.1002/adhm.201400164

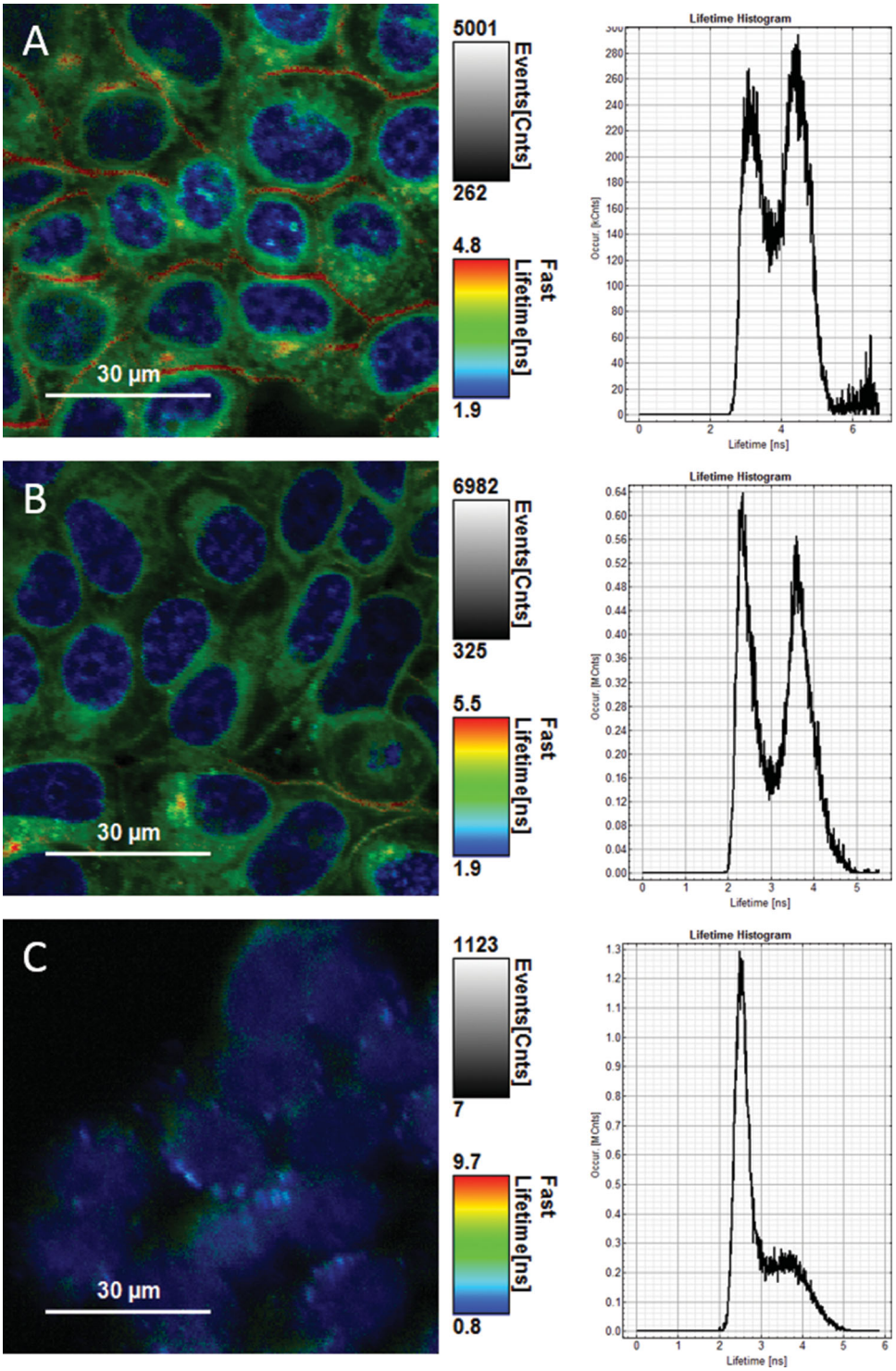

Figure 6. FLIM images and life-time histograms showing cell uptake of DOX/Gd-loaded stars using MCF-7 cells after A) 1 h, B) 5 h, and C) 24 h of incubation.

at 37 °C (Figure S18, Supporting Information). We observed a significant increase in the relaxivity (16.9 mM^{-1} s^{-1}) compared with free (no polymer) DO3A-NH_2-Gd (5.2 mM^{-1} s^{-1}). This result is in accord with our previous studies on the effect of the polymer architecture on the relaxivity of Gd.[4a] Interestingly, we observed a slight (5%–8%) increase in the relaxivity when DOX was conjugated to the stars as noted in **Table 3**. This slight influence of conjugated DOX can be attributed to the influence of DOX on the star cores giving a more rigid nanoparticle structure affecting isotropic rotational dynamics, increasing

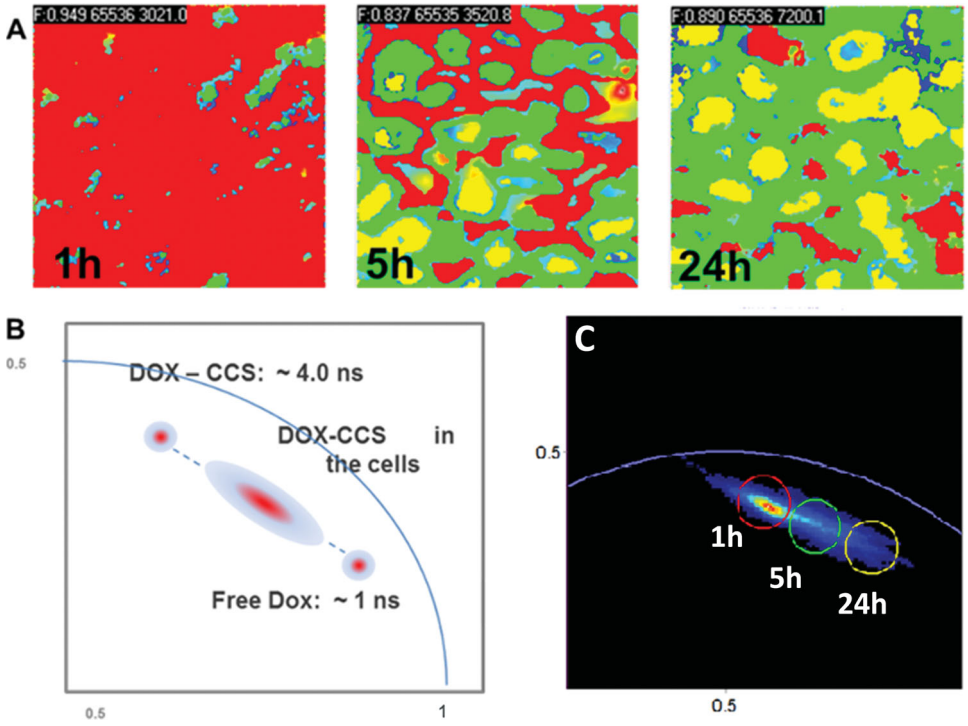

Figure 7. A) Fluorescence lifetime in MCF-7 live cells to monitor intercellular released of DOX from DOX/Gd-loaded stars; B) Schematic representation of phasor plot; C) Phasor plot derived from the FLIM images for MCF-7 breast cancer cells at different incubation times (1, 5, and 24 h) with DOX/Gd-loaded stars. Red ROI (region of interest) corresponds to the signal after 1 h of incubation; green ROI and orange ROI correspond to the signals after 5 and 24 h, respectively. Each ROI corresponds to different lifetimes of DOX in the cells corresponding to different amounts of DOX released from DOX/Gd-loaded stars.

τ_R and yielding ionic r_1 values in the order of several tens of mM^{-1} s^{-1},[23] Gd is placed in the star arms to give water accessibility in order to shorten water residence time (τ_m). Finally, we measured the relaxivity of stars after DOX release. In this experiment, the sample was incubated for 7 d in acidic water (pH 5.0) and then dialyzed against methanol to remove released DOX. UV–vis spectroscopy confirmed the complete release of DOX. Subsequently, the relaxivity was measured at 20 and 60 MHz (Figure S18, Supporting Information). Interestingly, the release of DOX had no effect on the relaxivity value of Gd.

3. Conclusions

We have described a simple and versatile synthetic route to theranostic nanoparticles. The nanoparticles were made exploiting sequential reactions with different amine functionality. The resultant star (nanoparticle) structure can be easily loaded with doxorubicin and Gd/DO3A. This structure presents significant formulation advantages, for example, this drug-loaded nanoparticle was easily (and reproducibly) regenerated after freeze-drying. The drug delivery efficacy of the nanoparticle vectors was complemented by highly effective MRI contrast capability.

Table 3. Relaxivity values for Gd-loaded star polymers.

Samples	r_1 at 20 MHz [mM^{-1} s^{-1}]	r_1 at 60 MHz [mM^{-1} s^{-1}]
Gd-CCS	16.9	14.3
DOX/Gd-DOX	18.8	14.7
DOX/Gd-DOX (after released of DOX)	19.5	15.7

Supporting Information

Supporting Information is available from the Wiley Online Library or from the author. Experimental details are included in the Supporting Information.

Acknowledgements

The authors thank the Nuclear Magnetic Resonance facility, Biomedical Imaging facility, and the Electron Microscope Unit at the Mark Wainwright Analytical Centre for helpful discussions and advice on the design of the experimental setup. The authors acknowledge the Australian Research Council (ARC) for funding in the form of a Discovery grant (DP110104251). In addition, the authors acknowledge significant research fellowship funding to C.B. (ARC-FT 120100096).

Received: March 25, 2014
Revised: May 27, 2014
Published online:

[1] a) S. J. Park, S.-H. Park, S. Cho, D.-M. Kim, Y. Lee, S. Y. Ko, Y. Hong, H. E. Choy, J.-J. Min, J.-O. Park, S. Park, *Sci. Rep.* **2013**, *3*, 3394; b) R. K. Jain, T. Stylianopoulos, *Nat. Rev. Clin. Oncol.* **2010**, *7*, 653;

c) P. P. Shanbhag, S. V. Jog, M. M. Chogale, S. S. Gaikwad, *Curr. Drug Delivery* **2013**, *10*, 357; d) S. A. Wickline, G. M. Lanza, *Circulation* **2003**, *107*, 1092; e) E. K.-H. Chow, D. Ho, *Sci. Transl. Med.* **2013**, *5*, 216rv214; f) O. M. Koo, I. Rubinstein, H. Onyuksel, *Nanomed. Nanotechnol.* **2005**, *1*, 193.

[2] a) S. Laurent, D. Forge, M. Port, A. Roch, C. Robic, L. V. Elst, R. N. Muller, *Chem. Rev.* **2008**, *108*, 2064; b) M. Mahmoudi, H. Hosseinkhani, M. Hosseinkhani, S. Boutry, A. Simchi, W. S. Journeay, K. Subramani, S. Laurent, *Chem. Rev.* **2010**, *111*, 253; c) J. Gao, H. Gu, B. Xu, *Acc. Chem. Res.* **2009**, *42*, 1097; d) H. B. Na, I. C. Song, T. Hyeon, *Adv. Mater.* **2009**, *21*, 2133; e) P. Hermann, J. Kotek, V. Kubicek, I. Lukes, *Dalton Trans.* **2008**, 23 3027.

[3] a) M. A. Perazella, *Clin. J. Am. Soc. Nephrol.* **2009**, *4*, 461; b) P. Caravan, J. J. Ellison, T. J. McMurry, R. B. Lauffer, *Chem. Rev.* **1999**, *99*, 2293.

[4] a) Y. Li, M. Beija, S. Laurent, L. V. Elst, R. N. Muller, H. T. T. Duong, A. B. Lowe, T. P. Davis, C. Boyer, *Macromolecules* **2012**, *45*, 4196; b) M. Beija, Y. Li, H. T. Duong, S. Laurent, L. V. Elst, R. N. Muller, A. B. Lowe, T. P. Davis, C. Boyer, *J. Mater. Chem.* **2012**, *22*, 21382; c) M. Milne, P. Gobbo, N. McVicar, R. Bartha, M. S. Workentin, R. H. Hudson, *J. Mater. Chem. B* **2013**, *1*, 5628; d) A. Gupta, T. J. Stait-Gardner, N. Kirby, W. S. Price, M. J. Moghaddam, *J. Mater. Chem. B* **2013**, 9, 1225; e) H. W. Zhang, L. Q. Wang, Q. F. Xiang, Q. Zhong, L. M. Chen, C. X. Xu, X. H. Xiang, B. Xu, F. Meng, Y. Q. Wan, D. Y. Deng, *Biomaterials* **2014**, *35*, 356; f) Y. Liu, N. Zhang, *Biomaterials* **2012**, *33*, 5363.

[5] a) P. Caravan, *Acc. Chem. Res.* **2009**, *42*, 851; b) M. O. Oyewumi, R. J. Mumper, *Bioconjugate Chem.* **2002**, *13*, 1328; c) Z. Cheng, D. L. Thorek, A. Tsourkas, *Angew. Chem Int. Ed.* **2010**, *49*, 346.

[6] B. Karagoz, L. Esser, H. T. Duong, J. S. Basuki, C. Boyer, T. P. Davis, *Polym. Chem.* **2014**, *5*, 350.

[7] a) S. Thakker, A. Rokhade, S. Abbigerimath, S. Iliger, V. Kulkarni, U. More, T. Aminabhavi, *Polym. Bull.* **2014**; b) K. Chaturvedi, S. K. Tripathi, A. R. Kulkarni, T. M. Aminabhavi, *J. Microencapsul.* **2013**, *30*, 356; c) K. S. Soppimath, T. M. Aminabhavi, A. R. Kulkarni, W. E. Rudzinski, *J. Controlled Release* **2001**, *70*, 1; d) R. C. Mundargi, V. R. Babu, V. Rangaswamy, P. Patel, T. M. Aminabhavi, *J. Controlled Release* **2008**, *125*, 193; e) S. A. Agnihotri, N. N. Mallikarjuna, T. M. Aminabhavi, *J. Controlled Release* **2004**, *100*, 5; f) S. Parveen, R. Misra, S. K. Sahoo, *Nanomed. Nanotechnol.* **2012**, *8*, 147.

[8] a) Y. Li, H. T. T. Duong, M. W. Jones, J. S. Basuki, J. Hu, C. Boyer, T. P. Davis, *ACS Macro Lett.* **2013**, *2*, 912; b) P. Theato, *J. Polym. Sci., Part A: Polym. Chem.* **2008**, *46*, 6677; c) N. Vogel, P. Théato, *Macro. Symposia* **2007**, *249–250*, 383; d) M. Eberhardt, R. Mruk, R. Zentel, P. Théato, *Europ. Polym. J.* **2005**, *41*, 1569; e) M. A. Gauthier, M. I. Gibson, H. A. Klok, *Angew. Chem.* **2009**, *48*, 48; f) C. Boyer, T. P. Davis, *Chem. Commun.* **2009**, 40, 6029.

[9] a) J. Liu, H. Duong, M. R. Whittaker, T. P. Davis, C. Boyer, *Macro. Rapid Commun.* **2012**, *33*, 760; b) H. T. T. Duong, F. Hughes, S. Sagnella, M. Kavallaris, A. Macmillan, R. Whan, J. Hook, T. P. Davis, C. Boyer, *Mol. Pharm.* **2012**, *9*, 3046.

[10] J. Ferreira, J. Syrett, M. Whittaker, D. Haddleton, T. P. Davis, C. Boyer, *Polym. Chem.* **2011**, *2*, 1671.

[11] C. Boyer, M. H. Stenzel, T. P. Davis, *J. Polym. Sci., Part A: Polym. Chem.* **2011**, *49*, 551.

[12] M. Beija, Y. Li, A. B. Lowe, T. P. Davis, C. Boyer, *Europ. Polym. J.* **2013**, *49*, 3060.

[13] a) A. W. Jackson, D. A. Fulton, *Chem. Commun.* **2010**, *46*, 6051; b) A. W. Jackson, C. Stakes, D. A. Fulton, *Polym. Chem.* **2011**, *2*, 2500.

[14] G. Kwon, M. Naito, M. Yokoyama, T. Okano, Y. Sakurai, K. Kataoka, *J. Controlled Release* **1997**, *48*, 195.

[15] J. S. Basuki, H. T. Duong, A. Macmillan, R. B. Erlich, L. Esser, M. C. Akerfeldt, R. M. Whan, M. Kavallaris, C. Boyer, T. P. Davis, *ACS Nano* **2013**, *7*, 10175.

[16] a) S. M. Sagnella, H. Duong, A. MacMillan, C. Boyer, R. Whan, J. A. McCarroll, T. P. Davis, M. Kavallaris, *Biomacromolecules* **2013**, *15*, 262; b) H. Guerrero-Cázares, S. Y. Tzeng, N. P. Young, A. O. Abutaleb, A. Quiñones-Hinojosa, J. J. Green, *ACS Nano* **2014**, *8*, 5141.

[17] a) Z. Zhang, X. Xiong, J. Wan, L. Xiao, L. Gan, Y. Feng, H. Xu, X. Yang, *Biomaterials* **2012**, *33*, 7233; b) L. Xiao, X. Xiong, X. Sun, Y. Zhu, H. Yang, H. Chen, L. Gan, H. Xu, X. Yang, *Biomaterials* **2011**, *32*, 5148.

[18] a) T.-G. Iversen, T. Skotland, K. Sandvig, *Nano Today* **2011**, *6*, 176; b) J. Voigt, J. Christensen, V. P. Shastri, *Proc. Natl. Acad. Sci. U.S.A.* **2014**; c) G. Sahay, D. Y. Alakhova, A. V. Kabanov, *J. Controlled Release* **2010**, *145*, 182.

[19] a) X. Dai, Z. Yue, M. E. Eccleston, J. Swartling, N. K. Slater, C. F. Kaminski, *Nanomed. Nanotechnol.* **2008**, *4*, 49; b) A. Kinoshita, T. Shah, M. M. Tangredi, D. K. Strickland, B. T. Hyman, *J. Biol. Chem.* **2003**, *278*, 41182; c) T. Liu, X. Li, Y. Qian, X. Hu, S. Liu, *Biomaterials* **2012**, *33*, 2521; d) G. Mikhaylov, U. Mikac, A. A. Magaeva, V. I. Itin, E. P. Naiden, I. Psakhye, L. Babes, T. Reinheckel, C. Peters, R. Zeiser, *Nat. Nanotechnol.* **2011**, *6*, 594.

[20] a) O. Hovorka, V. Subr, D. Vetvicka, L. Kovar, J. Strohalm, M. Strohalm, A. Benda, M. Hof, K. Ulbrich, B. Rihova, *Eur. J. Pham. Biopharm.* **2010**, *76*, 514; b) G.-J. Bakker, V. Andresen, R. M. Hoffman, P. Friedl, *Methods in Enzymology*, *504*, (Ed: P. M. Conn), Academic Press, USA **2012**, 109; c) H. T. T. Duong, F. Hughes, S. Sagnella, M. Kavallaris, A. MacMillan, R. Whan, J. Hook, T. P. Davis, C. Boyer, *Mol. Pharm.* **2012**, *9*, 3046.

[21] J. A. Broussard, B. Rappaz, D. J. Webb, C. M. Brown, *Nat. Protoc.* **2013**, *8*, 265.

[22] a) D. M. Jameson, E. Gratton, R. D. Hall, *Appl. Spectrosc. Rev.* **1984**, *20*, 55; b) G. I. Redford, R. M. Clegg, *J. Fluoresc.* **2005**, *15*, 805; c) M. A. Digman, V. R. Caiolfa, M. Zamai, E. Gratton, *Biophys. J.* **2008**, *94*, L14.

[23] a) A. J. L. Villaraza, A. Bumb, M. W. Brechbiel, *Chem. Rev.* **2010**, *110*, 2921; b) D. A. Fulton, M. O'Halloran, D. Parker, K. Senanayake, M. Botta, S. Aime, *Chem. Commun.* **2005**, 4, 474.